Current Distance Relations for Fiber Stimulation With Pointsources

Frank Rattay

***Abstract*—The following results are based on computer simulations and on activating function analysis. In the near field, denervated muscle fibers as well as nerve fibers with a sealed ending are easier to stimulate in the central region than with electrodes close to the end. When electrode-fiber distance is increased, the electrode location for optimal stimulation efficacy shifts from a central position to a region beyond the fiber end for cathodic stimulation and to a position above the terminating part of the fiber for anodic currents. The phenomenon becomes more pronounced with increasing distance between the electrode and fiber axis, because in the far field, the current–distance relation changes from quadratic to cubic, whereas stimulation at the fiber end obeys a rather constant quadratic law.**

***Index Terms*—Activating function, microelectrode, pointsource, threshold current.**

I. Introduction

REHABILITATION of patients with long-term denervated muscles by electrical stimulation needs extensive training with the application of strong stimulation currents [1], [2]. Apart from transcutaneous stimulation, human denervated muscle fibers are sometimes excited with needle electrodes [3]. In both cases, the relation between threshold current and electrode positions relative to target fibers should be explored in order to optimize clinical stimulation protocols. In Sections II and III, we analyze pointsource stimulation of straight fibers in a homogeneous medium as a first approximation for excitation in the vicinity of small electrodes. The proposed method for a 1-D cable model with a sealed end can also be extended to nerve fibers with nonbifurcating endings (e.g., stimulation of the auditory nerve with cochlea implants [4], [5]) or axon terminal stimulation [6], [7].

The excitability of long-term denervated muscles is critically determined by the actual biological conditions of the diverse types of muscle fibers [8], [9]. In contrast to healthy muscle fibers [10], modeling work that considers membrane excitation for different states of denervation is still lacking [11]. However, excitation analysis is easy if a uniformed membrane and constant diameter can be assumed, resulting in a close relationship between 1) a simple form of the activating function, 2) subthreshold transmembrane voltage maxima, and 3) spike initiation regions.

Manuscript received August 18, 2006; revised July 17, 2007.

The author is with the Institute for Analysis and Scientific Computing at the Vienna University of Technology, TU-BioMed, Wiedner Hauptstr. 8-10/101, Vienna A-1040, Austria (e-mail: frank.rattay@tuwien.ac.at).

Digital Object Identifier 10.1109/TBME.2008.915676

Previous computer simulation studies of the transcutaneously stimulated human thigh revealed the existence of several spike initiation zones in a single denervated muscle fiber [12]. Especially in deeper regions, action potentials are hard to evoke within the central part, even with pulse amplitudes up to 100 V. In such surface electrode applications, spike initiation is expected to occur mainly at the fiber endings [12], [13]. For stimulation with pulses from monopolar pointsources, we will show a similar effect in the far field, in contrast, however, to the situation in the near field, where the fiber remained more excitable in its central parts.

II. Methods

Fiber excitation is modeled according to Adrian and Henneberg as a Hodgkin Huxley-type compartment model that includes a passive element for the current flow into the tubular system [14], [15] (for details, see [16]). The current relation along the fiber is

$$i_m + i_t = c\frac{\partial V}{\partial t} + i_{\text{ion}} + i_t = \frac{d}{4\rho_i}\left(\frac{\partial^2 V}{\partial x^2} + \frac{\partial^2 V_e}{\partial x^2}\right) \tag{1}$$

with

$$\frac{\partial V_t}{\partial t} = \frac{1}{c_t}\left(\frac{V - V_t}{r_a} - (V_t - V_{\text{rest}})\cdot g_t\right) \text{ and } i_t = \frac{V - V_t}{r_a} \tag{1a}$$

where i_m, i_{ion}, and i_t denote total current and ion currents across the membrane, as well as tubular current flow, respectively; c is the membrane capacity; d is the fiber diameter; ρ_i is intracellular resistivity; r_a is tubular system resistance; and g_t is the tubular membrane conductance. Membrane voltage V and the extracellular potential V_e as well as their derivatives enter the model as functions of the fiber's length coordinate x. With a constant compartment length Δx, the numerical form of (1) results in a set of ordinary differential equations which reads for the central compartments as

$$\frac{dV_n}{dt} = -\frac{(i_{\text{ion},n} + i_t)}{c} + \frac{d}{4c\cdot\rho_i} \times \left[\frac{V_{n+1} - 2\cdot V_n + V_{n-1}}{\Delta x^2} + \frac{V_{e,n+1} - 2\cdot V_{e,n} + V_{e,n-1}}{\Delta x^2}\right] \tag{2}$$

and

$$\frac{dV_1}{dt} = -\frac{(i_{\text{ion},n} + i_t)}{c} + \frac{d}{4c\Delta x \cdot \rho_i} \times \left[\frac{V_2 - V_1}{\Delta x} + \frac{V_{e,2} - V_{e,1}}{\Delta x}\right] \tag{2a}$$

$$\frac{dV_N}{dt} = -\frac{(i_{\text{ion},n} + i_t)}{c} + \frac{d}{4c\Delta x \cdot \rho_i} \times \left[\frac{V_{N-1} - V_N}{\Delta x} + \frac{V_{e,N-1} - V_{e,N}}{\Delta x}\right] \tag{2b}$$

at the endings. This means that the activating function [7], [17], [18] for the central part becomes

$$f_n = \frac{d}{4c \cdot \rho_i} \cdot \frac{V_{e,n+1} - 2 \cdot V_{e,n} + V_{e,n-1}}{\Delta x^2}. \tag{3}$$

With $\Delta x \to 0$, f is proportional to the second derivative of the extracellular voltage

$$f(x) = \frac{d}{4\rho_i c}\frac{\partial^2 V_e}{\partial x^2} \tag{4}$$

whereas at the endings

$$f_1 = \frac{d}{4c\Delta x \cdot \rho_i}\frac{V_{e,2} - V_{e,1}}{\Delta x} \tag{5a}$$

$$f_N = \frac{d}{4c\Delta x \cdot \rho_i}\frac{V_{e,N-1} - V_{e,N}}{\Delta x} \tag{5b}$$

the stimulating influence depends on the first derivative of the extracellular voltage. Note that the terminal activating function is proportional to the first difference quotient of V_e, weighted by the compartment length by $1/\Delta x$.

For a monopolar pointsource in an infinite homogeneous isotropic medium with resistivity ρ_e, the external potential along the fiber is

$$V_e = \frac{\rho_e . I_{\text{el}}}{4\pi . r} = \frac{\rho_e . I_{\text{el}}}{4\pi}\left((x - x_{\text{el}})^2 + z_{\text{el}}^2\right)^{-0.5} \tag{6}$$

where the fiber axis is the x-axis of the coordinate system, x_{el} and z_{el} are the electrode coordinates, and I_{el} is the pointsource current.

With the fiber originating at $x = 0$, we obtain from the continuous form of V_e

$$f_1 \approx \frac{d}{4c\Delta x \cdot \rho_i}\frac{\rho_e . I_{\text{el}}}{4\pi} x_{\text{el}}\left(x_{\text{el}}^2 + z_{\text{el}}^2\right)^{-3/2} \tag{7}$$

and

$$f_n \approx \frac{d}{4c\rho_i}\frac{\rho_e . I_{\text{el}}}{4\pi}\left(2(x_n - x_{\text{el}})^2 - z_{\text{el}}^2\right) \times \left((x_n - x_{\text{el}})^2 + z_{\text{el}}^2\right)^{-5/2}. \tag{8}$$

Note that the sign of f is important, as fiber regions with $f > 0$ are candidates for spike initiations.

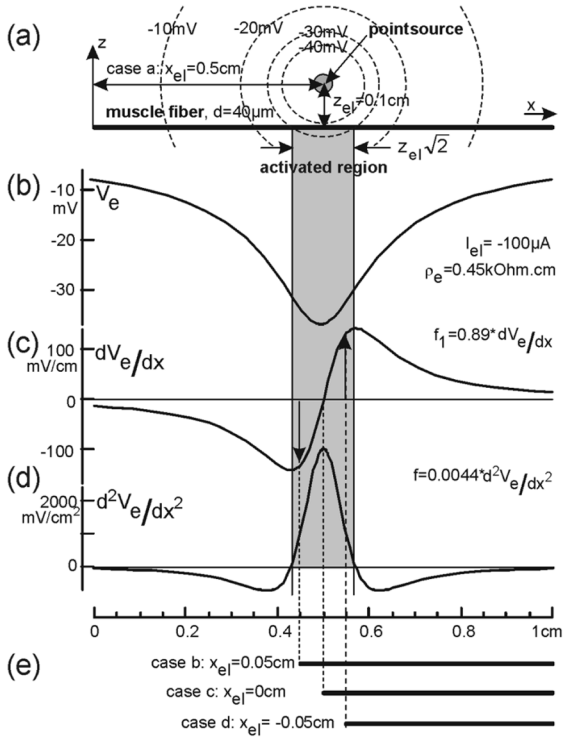

Fig. 1. Geometry, electrical field, and activating functions for pointsource stimulation of a straight fiber. Cutting a front part of the fiber as in (e) results in a change of the terminal activating function as indicated by arrows in (c), whereas the main equation (2) for all of the other compartments gets the same driving input as before cutting. f_1 and f depend on fiber parameters; standard values used $d = 0.0040$ cm, $\rho_i = 0.173$ kΩ.cm, $c = 1.3$ μF/cm^2, $\Delta x = 0.0050$ cm.

III. Results

For stimulation with monophasic pulses, the subthreshold response of every compartment is driven by the input of either the terminal [(2a), (2b)] or central form (2) of the activating function. The individual f contributions, however, critically change with pointsource position. In the first investigation, the pointsource is moved along the fiber from a central position (case a) to the left side until an electrode position shortly beyond the fiber end (case d). Fig. 1(a)–(d) shows the situation for case a ($x_{\text{el}} = 0.5$ cm, $z_{\text{el}} = 0.1$ cm), with corresponding V_e and its derivatives for $I_{\text{el}} = -100$ μA and $\rho_e = 0.45$ kΩ.cm (typical resistivity in a long-term denervated human thigh).

With the assumptions of Fig. 1(a) membrane voltage $V(x)$ of a muscle fiber ($d = 40$ μm, $\Delta x = 50$ μm) is affected mainly by the central activating function values, although f_1 is similar in size with the peak value of f at $x = x_{\text{el}}$. This f_1 value is too small to dominate the subthreshold response because it mainly drives just one single compartment, nevertheless inducing hyperpolarization of the fiber end [Fig. 2(a)].[1] This "negative" f_1 influence increases by a factor of 9 when the electrode is moved parallel to the fiber to $x_{\text{el}} = 0.05$ cm [Fig. 2(b)] and reduces

[1]Note that the terminal activating functions f_1 and f_N depend on Δx [5(a) and 5(b)] and, consequently, for example, halving Δx causes a doubling of the f_1 value. Regardless of this fact, as long as Δx is small enough, its actual magnitude cannot remarkably influence the computed membrane voltage.

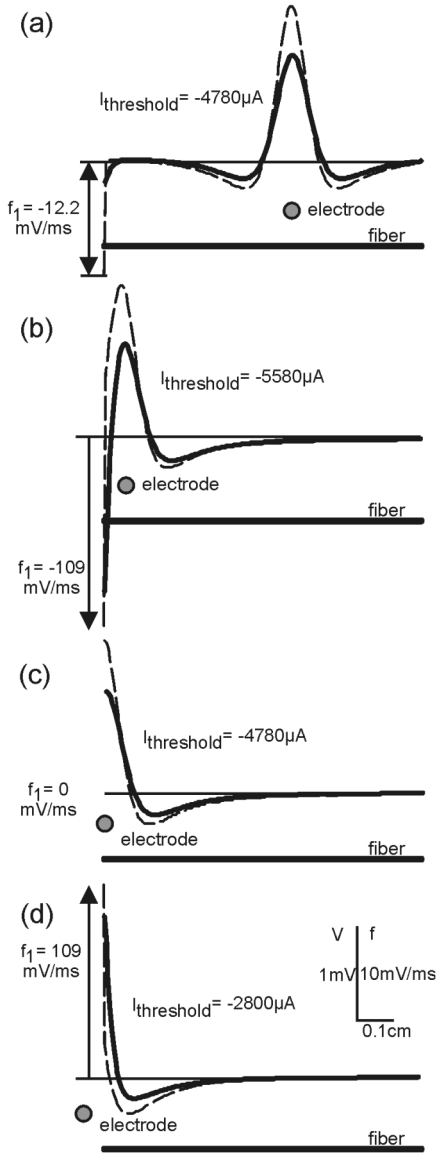

Fig. 2. Activating functions (dashed lines) and subthreshold membrane voltages (full lines) for cathodic pointsource stimulation at the end of a -100-μA, 100-μs pulse. As in Fig. 1, the electrode has a constant distance from the fiber axis (1 mm), the right fiber end is not shown; electrode x-distance from left fiber end is 5 mm, 0.5 mm, 0 and -0.5 mm (a-d). Note the negative f_1 value in a and b causes a hyperpolarization of the fiber ending.

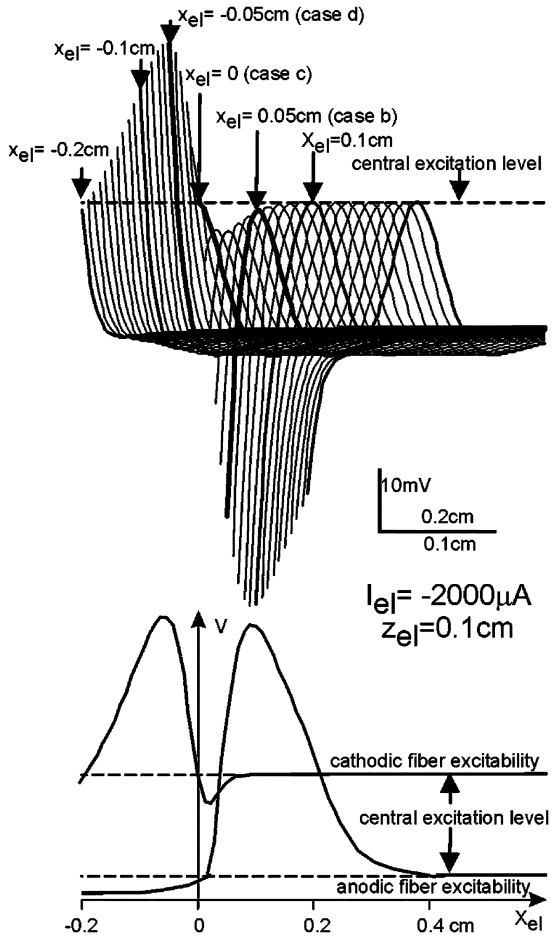

Fig. 3. Far-field membrane voltage as a function of electrode displacement along the fiber axis. Forty-membrane voltage profiles at the end of the 100-μs pulse are shifted in the x-direction (data as in Fig. 2 but with 20 times stronger stimulus amplitude). The curves corresponding to b-d from Fig. 2 (thick lines, marked by arrows) have not changed their shapes. Curve details lost due to low picture resolution remain negligible as the figure demonstrates the principal relation between the electrode position and the maximum and minimum values of the voltage profiles: Cathodic and anodic fiber excitability (lower diagram) are related to the envelopes of these shifted voltage profiles; shifting demands for two horizontal scales: narrow scaling (2-mm bar) belongs to the single V profiles and the 1-mm bar belongs to envelopes for $x > 0$ in the upper traces. The starting points of the V curves are strongly affected by f_1 and (because of cathodic stimulation) appear as a mirror picture of Fig. 1(c).

excitation in comparison to case a, implying that the maximum value of V becomes smaller and, consequently, threshold current is increased. Moving the electrode above the fiber ending (case c, $x_{\rm el} = 0$) needs the same threshold current as central fiber stimulation (case a) because $f_1 = 0$ at $x_{\rm el} = 0$. Moving the electrode to the left side causes a change in sign of f_1 from $-$ to $+$ after passing the fiber end and, surprisingly, the fiber becomes maximally excitable for a position beyond the fiber end (close to case d), where both f_1 and f have rather large positive values.

Fig. 3 demonstrates the polarity effect of f_1 in more detail. Stimulation with a -2000-μA, 100-μs pulse causes higher membrane voltages but still evokes substhreshold responses. In 40 discrete steps, the electrode is moved from $x_{\rm el} = 0.2$ cm to the left side to $x_{\rm el} = -0.2$ cm. The membrane voltage curves (which are horizontally shifted) cannot reach the theoretical central excitation level as a consequence of negative f_1 values for $x_{\rm el} > 0$, which is especially seen in the region between $x_{\rm el} = 0$ and $x_{\rm el} = 0.06$ cm. Due to these horizontal V curve shifts, the upper envelope of the V curves needs some horizontal corrections for $x_{\rm el} > 0$ in order to represent the fiber excitability as a function of $x_{\rm el}$ (Fig. 3, lower part). It is of note that cathodic and—even more pronounced—anodic excitability reaches remarkable peak values when the electrode is positioned within a displacement range of $+/-2$ mm near the fiber end.

A. Current Distance Relations in Radial Direction

Setting, for example, $x_{\rm el} = z_{\rm el}/2$ in (7) demonstrates the quadratic relationship between f_1 and the distance between the electrode center and fiber axis $f_1 = -1.2/z_{\rm el}^2$ for $I_{\rm el} = -100$ μA when using our standard parameter set

TABLE I
RADIAL CURRENT DISTANCE RELATIONS FOR CATHODIC MUSCLE FIBER THRESHOLDS

	central activation			terminal activation			
z_{el} [cm]	I_{el} [μA]	$\frac{I_{el}(z_{el})}{I_{el}(z_{el}/2)}$	f [mV/ms]	I_{el} [μA]	$\frac{I_{el}(z_{el})}{I_{el}(z_{el}/2)}$	f_1 [mV/ms]	
0.8	1800000	7.79	559	211000	4.05	3824	
0.4	231000	7.45	572	52000	4.85	3752	far
0.2	31000	6.49	616	10700	3.96	3115	field
0.1	4780	5.31	757	2700	3.71	3179	$z_{el}>\lambda$
0.05	900	4.13	1125	727	3.35	3497	
0.025	218	3.30	2066	217	2.81	4230	near
0.0125	66	2.54	4140	77	2.48	6012	field
0.00625	26		13045	31		9682	$z_{el}<\lambda$

Terminal electrode thresholds current I_{el} and activating functions f_1 are calculated for $x_{el} = -z_{el}/2$. Note the moderate distance dependence of f_1, because at threshold f_1 is related to the injected current at the fiber terminal that is needed to generate an action potential. Non-constant values in the last columns are caused by the external stimulation of the central fiber compartments.

with $\Delta x = 0.0050$ cm and the "classical" units: millivolts, centimeters, milliseconds, kilo-ohms.cm, etc. The maximum contribution of the central activating function appears at $x = x_{\rm el}$ which (in our example) results from (8) in $f = 0.016/z_{\rm el}^3$. Current flow within the fiber smoothes membrane voltage responses due to irregularities of f along the fiber and prevents a simple relation between the maximum f value $f_{\max}$ and threshold current $I_{\rm threshold}$. However, the axial current flow is negligible if f is close to $f_{\max}$ within an interval considerably longer than the fiber's length constant λ. Therefore, the cubic distance relation of f approximates the central threshold current behavior better with increasing distances, resulting finally in an 8-fold threshold current for doubled distance (compare Table I, column 3).[2] When the most stimulated region shrinks in length, the f contribution, which is related to an injected current to every compartment, loses a fraction as current flow to the neighboring sections instead of loading the membrane capacitor, thus generating a full local membrane voltage increase. At the border of far and near field ($z_{\rm el} = \lambda = 330$ μm for our standard data), a 50% decrease in $z_{\rm el}$ requires approximately doubled f and 1/4 of $I_{\rm threshold}$—and this trend of deviation from the cubic relation continues for shorter distances (Table I, columns 3 and 4).

In contrast to central stimulation, excitation at the fiber end has an almost quadratic current–distance relation for every $z_{\rm el}$ in the far field. In the far field, the advantage of cathodic stimulation of distal activation shrinks with distance and vanishes at about $z_{\rm el} = 250$ μm (Table I, Fig. 4). This phenomenon is a consequence of the different threshold increase factors (when electrode-fiber distance is doubled) for central and distal stimulation: central activation dominates the situation as soon as this factor (third column of Table I) falls below 4. On the other hand, distal excitation in the far field can increase its efficiency for well-placed electrodes. This is demonstrated for $z_{\rm el} = 0.4$ cm, where cathodic terminal excitation exceeds the central stimulation response for a 1.4-cm-long region situated in front of the fiber (Fig. 5). Shifting the electrode in 0.1-cm steps results in a stronger excitation at $x_{\rm el} = -0.3$ cm instead of the suggestion to use $x_{\rm el} = -z_{\rm el}/2 = -0.2$ cm. Due to the extremely reduced support from the rather small values of f, the central component becomes negligible. This suggests using the $x_{\rm el}$ value of the f_1 maximum for this case or for even larger $z_{\rm el}$, that is $x_{\rm el} = -z_{\rm el}/\sqrt{2}$ (compare the upward arrow in Fig. 1(c) at $x_{\rm el} = -z_{\rm el}/2$, where we find a supporting positive f value of similar size in Fig. 1(d). This effect also explains the good choice for $z_{\rm el} = 0.1$ cm as demonstrated in Fig. 3).

[2]Threshold current of the pointsource is found by an iterative procedure with the full set of (1a), (2), (2a), (2b) until an action potential is just generated.

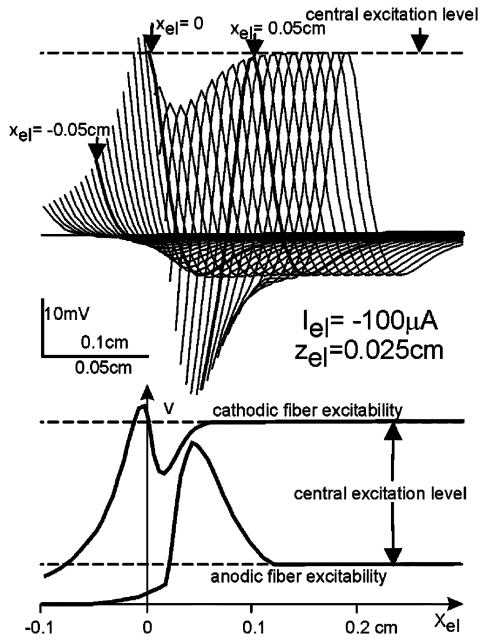

Fig. 4. Near-field membrane voltage as function of electrode displacement along the fiber axis. Same display format as in Fig. 3, shows a narrow region where terminal excitation exceeds the central excitability with cathodic pulses. Anodic terminal excitation effects are more pronounced compared to central excitability, but for all electrode positions, cathodic thresholds are lower than anodic ones.

IV. DISCUSSION

Most of the following similarities and dissimilarities in the far and near field can be found by comparing Figs. 3 and 4 (note their different x-scaling): 1) the excitability curves, both cathodic and anodic keep their characteristic shape and 2) for a specific $z_{\rm el}$, anodic and cathodic peaks are of similar size; 3) both peaks, however, decrease relative to the central excita-

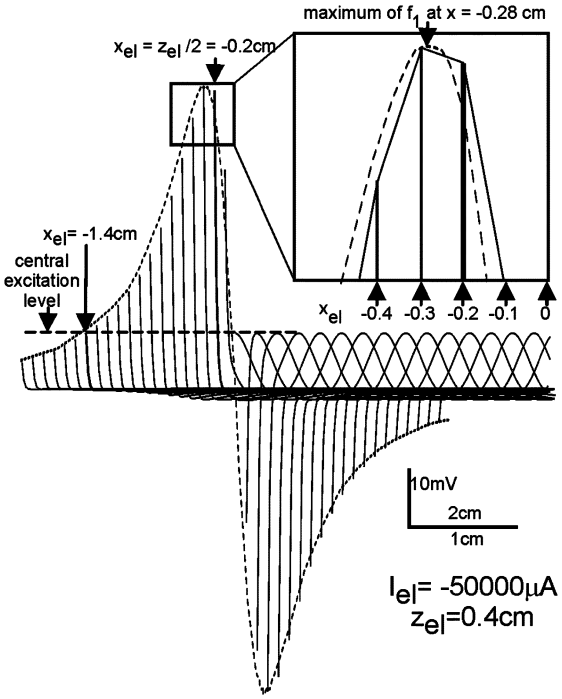

Fig. 5. Membrane voltage profiles for $z_{\rm el} = 4$ mm and distal activating function f_1 (dashed line). Enlarged insert: electrode placement for maximum excitation is close to the theoretical value predicted by f_1; there is a rather small supporting contribution from the central activating function at $x_{\rm el} = -0.2$ cm (thick line, exceeding the dashed line values of f_1). Dashed line f_1 scaled to a maximum of V.

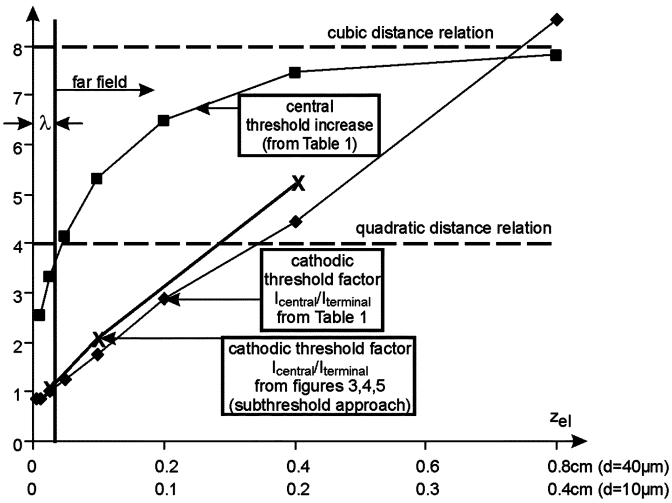

Fig. 6. Summary of current distance results for muscle fibers with 10- and 40-μm diameters stimulated with cathodic 100-μs pulses (increase factors for doubling electrode distance $z_{\rm el}$). In the far field, central stimulation changes from a quadratic to a cubic excitation–distance relation, which gradually increases the benefit for terminal stimulation as shown by the threshold factor marked by x (from subthreshold data extrapolation) and diamonds (calculated thresholds from Table I).

tion levels when $z_{\rm el}$ is reduced; 4) the cathodic excitation level at $x_{\rm el} = 0$ is the same as for an electrode with the same $z_{\rm el}$ positioned above the center of the fiber; 5) for small $z_{\rm el}$, the $x_{\rm el} = 0$ position is the best suited for cathodic terminal stimulation as excitability decreases in both x-directions as soon as $z_{\rm el}$ falls below 250 μm (Table I); 6) in both the near and the far field, there is a less excitable region for small positive $x_{\rm el}$ values and cathodic stimulation but 7) a rather large region with good anodic excitability; 8) in the far field, $x_{\rm el} = -z_{\rm el}/2$ is a good guess for efficient electrode position but 9) for larger distances $(z_{\rm el} > 0.3\,{\rm cm})$ the most efficient position is shifted more toward $x_{\rm el} = -z_{\rm el}/\sqrt{2}$, where f_1 has its maximum (Fig. 5); 10) the region where central cathodic excitation is somewhat reduced is rather distance independent $(0 < x_{\rm el} < 0.05\,{\rm cm})$ as it is related to the λ-dependent voltage course for terminal current injection, whereas 11) the region where distal excitability exceeds the central one rapidly increases with $z_{\rm el}$ [0.2 cm for $z_{\rm el} = 0.1$ cm, 1.4 cm for $z_{\rm el} = 0.4$ cm– comp. Figs. 3 and 5].

Apart from a lot of other effects, human muscle fiber denervation also causes diameter reduction, resulting in diameters within the 10–40 μm range. For the 10-μm diameter fiber, we obtain quite the same numerical values as for the 40-μm diameter fiber in differential equations (2), (2a), and (2b) as well as for their input V_e by halving both the geometry values (Δx, $x_{\rm el}$, and $-z_{\rm el}$) and electrode current $I_{\rm el}$. This "same input—same output" principle holds for arbitrary diameters and causes, for example, a change in the scaling of the x-axis only in Fig. 6. In order to use Table I for diameter d (in micrometers), we need a correction factor $correct = \sqrt{d/40}$ in columns 1, 2, and 5. Also, Figs. 2–5 are valid when $correct$ is applied to x scaling and $I_{\rm el}$.

When current flow into the tubular system is suppressed, the membrane potential becomes a bit more depolarized, causing, for example, vertical enlargements of all curves in Figs. 3–5 in the lower percent range, without altering the overall shape of any curve in a qualitative way (tested but not shown). Furthermore, these typical envelopes as in the presented figures were found (results not shown) with the original Hodgkin Huxley model data. Therefore, we conclude that the main results are also correct for the subthreshold behavior of nonbifurcating unmyelinated nerve fibers, and can be used to predict the spike initiation site as well as anodic and cathodic threshold relations and their dependence on pointsource position.

Long-term denervated human muscles are currently trained with large surface electrodes [2], [9]. Here, it is not possible to find an electrode arrangement that optimizes the simultaneous stimulation of large fiber populations in different muscles by considering the supporting effects of central and terminal stimulation for every fiber because their myotendon junctions are not concentrated within small regions. In such cases, efficient stimulation of target muscles needs strong terminal activating functions within the whole region of fiber endings when deeper muscles cannot be activated by spike initiation in central compartments. However, for example, muscle activation with a distributed system of small implanted electrodes can be approximated by the presented pointsource stimulation model.

Considering efficient pointsource positions, we have shown that the combined contributions of central and terminal activating functions are of crucial importance in many cases of denervated muscle fibers. Biopsies of human long-term denervated muscles show severe disarrangements in muscle tissue [9], which led to the assumption of an isotropic medium in this study. Nonisotropic cases, corresponding to the healthy

muscle or to the recovery by training [9], can be simulated by a coordinate transformation in the x-direction, resulting in the same characteristic features for terminal and central stimulation. Moreover, the presented scheme is not restricted to pointsource stimulation or electrical constraints of the extracellular medium. Incorporating the generalized form of the activating function [7], [19] into the proposed method, it can be easily applied to arbitrary cell shapes, and this way, it will be a valuable tool for analyzing neural tissue stimulation with microelectrodes.

REFERENCES

[1] K. F. Eichhorn, W. Schubert, and E. David, "Maintenance, training and functional use of denervated muscles," *J. Biomed. Eng.*, vol. 6, pp. 205–211, 1984.

[2] H. Kern, S. Salmons, W. Mayr, K. Rossini, and U. Carraro, "Recovery of long-term denervated human muscles induced by electrical stimulation," *Muscle Nerve*, vol. 31, pp. 98–101, 2005.

[3] C. Hofer, C. Forstner, M. Mödlin, H. Jager, W. Mayr, and H. Kern, "In vivo assessment of conduction velocity and refractory period of denervated muscle fibers," *Artif. Organs*, vol. 29, pp. 436–439, 2005.

[4] J. T. Rubinstein, "Axon termination conditions for electrical stimulation," *IEEE Trans. Biomed. Eng.*, vol. 40, no. 7, pp. 654–63, Jul. 1993.

[5] F. Rattay, P. Lutter, and H. Felix, "A model of the electrically excited human cochlear neuron. I. contribution of neural substructures to the generation and propagation of spikes," *Hear. Res.*, vol. 153, pp. 43–63, 2001.

[6] B. Katz and R. Miledi, "A study of synaptic transmission in the absence of nerve impulses," *J. Physiol.*, vol. 192, pp. 407–436, 1967.

[7] F. Rattay, "The basic mechanism for the electrical stimulation of the nervous system," *Neurosci.*, vol. 89, pp. 335–346, 1999.

[8] E. I. Dedkov, A. B. Borisov, and B. M. Carlson, "Dynamics of postdenervation atrophy of young and old skeletal muscles: Differential responses of fiber types and muscle types," *J. Gerontol. A. Biol. Sci. Med. Sci.*, vol. 58, pp. 984–991, 2003.

[9] H. Kern, S. Boncompagni, K. Rossini, W. Mayr, G. Fano, M. E. Zanin, M. Podhorska-Okolow, F. Protasi, and U. Carraro, "Long-term denervation in humans causes degeneration of both contractile and excitation-contraction coupling apparatus, which is reversible by functional electrical stimulation (FES): A role for myofiber regeneration?," *J. Neuropathol. Exp. Neurol.*, vol. 63, pp. 919–931, 2004.

[10] W. Wallinga, S. L. Meijer, M. J. Alberink, M. Vliek, E. D. Wienk, and D. L. Ypey, "Modelling action potentials and membrane currents of mammalian skeletal muscle fibres in coherence with potassium concentration changes in the T-tubular system," *Eur. Biophys. J.*, vol. 28, pp. 317–329, 1999.

[11] M. Reichel, W. Mayr, and F. Rattay, "Simulation of resting membrane potential change in denervated muscle fiber," in *Proc. 5th Annu. Conf. Int. Functional Electrical Stimulation Society*, Aalborg, Denmark, pp. 249–252.

[12] F. Rattay, M. Reichel, J. Martinek, I. Persy, S. Resatz, and W. Mayr, "Functional electrical stimulation of denervated skeletal muscles: A modeling study," in *Proc. Eng. Med. Biol. Soc., 25th Annu. Int. Conf. Cancun*, Mexico, 2003, pp. 1553–1556.

[13] J. Martinek, M. Reichel, F. Rattay, and W. Mayr, "Analysis of calculated electrical activation of denervated muscle fibres in the human thigh," *Artif. Organs*, vol. 29, pp. 444–447, 2005.

[14] R. H. Adrian and L. D. Peachey, "Reconstruction of the action potential of frog sartorius muscle," *J. Physiol.*, vol. 235, pp. 103–131, 1973.

[15] K. A. Henneberg and F. A. Roberge, "Simulation of propagation along an isolated skeletal muscle fiber in an isotropic volume conductor," *Annu. Biomed. Eng.*, vol. 25, pp. 5–28, 1997.

[16] M. Reichel, "Funktionelle Elektrostimulation denervierter Skelettmuskulatur -Modellbildung und Simulation," (in German) Ph.D. dissertation, Inst. Anal. Scientif. Comput., Vienna Univ. Technol., Vienna, Austria, 1999.

[17] F. Rattay, "Analysis of models for extracellular fiber stimulation," *IEEE Trans. Biomed. Eng.*, vol. 36, no. 7, pp. 676–682, Jul. 1989.

[18] F. Rattay, *Electrical Nerve Stimulation*. New York: Springer, 1990.

[19] F. Rattay, "Analysis of the electrical excitation of CNS neurons," *IEEE Trans. Biomed. Eng.*, vol. 45, no. 6, pp. 766–772, Jun. 1998.

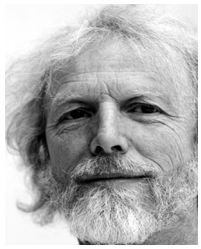

Frank Rattay received the Dr.Tech. and Dr.Sci. degrees from the Vienna University of Technology, Vienna, Austria, in 1980 and 1995, respectively, and the Dr.Med. science degree from the Vienna University of Medicine, Vienna, in 2006.

Currently, he is a Professor of Modeling and Simulation in techniques and science and for biophysics with the Institute of Analysis and Scientific Computing, Vienna University of Technology. He is also the Chair of the Association for Biomedical Engineering at the Vienna University of Technology (TU-BioMed). In 1986, he introduced the concept of the activating function, which explains the influence of an externally applied electric field on a target neuron.

Dr. Rattay is a Founding Member of the International Functional Electrical Stimulation Society and was the main organizer and President of the First World Congress on Neuroinformatics in Vienna in 2001.